Benchmarking viromics: An *in silico* evaluation of metagenome-enabled estimates of viral community composition and diversity

Simon Roux [Corresp., 1] , Joanne B Emerson [1] , Emiley A Eloe-Fadrosh [2] , Matthew B Sullivan [Corresp. 1, 3]

[1] Department of Microbiology, Ohio State University, Columbus, Ohio, United States

[2] Joint Genome Institute, Department of Energy, Walnut Creek, California, United States

[3] Department of Civil, Environmental and Geodetic Engineering, Ohio State University, Columbus, Ohio, United States

Corresponding Authors: Simon Roux, Matthew B Sullivan
Email address: roux.8@osu.edu, mbsulli@gmail.com

Background. Viral metagenomics (viromics) is increasingly used to obtain uncultivated viral genomes, evaluate community diversity, and assess ecological hypotheses. While viromic experimental methods are relatively mature and widely accepted by the research community, robust bioinformatics standards remain to be established. Here we used *in silico* mock viral communities to evaluate the viromic sequence-to-ecological-inference pipeline, including (*i*) read pre-processing and metagenome assembly, (*ii*) thresholds applied to estimate viral relative abundances based on read mapping to assembled contigs, and (*iii*) normalization methods applied to the matrix of viral relative abundances for alpha and beta diversity estimates. **Results.** Tools specifically designed for metagenomes, specifically metaSPAdes and MEGAHIT, were the most effective at assembling viromes. Read pre-processing, such as partitioning, had virtually no impact on assembly output, but may be useful when hardware is limited. Viral populations with 2–5x coverage typically assembled well, whereas lesser coverage led to fragmented assembly. Strain heterogeneity within populations hampered assembly, especially when strains were closely related (average nucleotide identity, or ANI ≥ 97%) and when the most abundant strain represented < 50% of the population. Viral community composition assessments based on read recruitment were generally accurate when the following thresholds for detection were applied: (*i*) ≥ 10kb contig lengths to define populations, (*ii*) coverage defined from reads mapping at ≥ 90% identity, and (*ii*) ≥ 75% of contig length with ≥ 1x coverage. Finally, although data are limited to the most abundant viruses in a community, alpha and beta diversity patterns were robustly estimated (±10%) when comparing samples of similar sequencing depth, but more divergent (up to 80%) when sequencing depth was uneven across the dataset. In the latter cases, the use of normalization methods specifically developed for metagenomes provided the best estimates.

Conclusions. These simulations provide benchmarks for selecting analysis cut-offs and establish that an optimized sample-to-ecological-inference viromics pipeline is robust for making ecological inferences from natural viral communities. Continued development to better accessing RNA, rare, and/or diverse viral populations and improved reference viral genome availability will alleviate many of viromics remaining limitations.

Benchmarking viromics: An *in silico* evaluation of metagenome-enabled estimates of viral community composition and diversity

Simon Roux[1,†,*], Joanne B. Emerson[1], Emiley A. Eloe-Fadrosh[2], Matthew B. Sullivan[1,3,*]

[1] Department of Microbiology, The Ohio State University, Columbus, OH, USA
[2] United States Department of Energy Joint Genome Institute, Lawrence Berkeley National Laboratory, Walnut Creek, CA, USA
[3] Department of Civil, Environmental and Geodetic Engineering, The Ohio State University, Columbus OH, USA

[†] Current address: United States Department of Energy Joint Genome Institute, Lawrence Berkeley National Laboratory, Walnut Creek, CA, USA
[*] to whom correspondence should be addressed

Abstract

Background. Viral metagenomics (viromics) is increasingly used to obtain uncultivated viral genomes, evaluate community diversity, and assess ecological hypotheses. While viromic experimental methods are relatively mature and widely accepted by the research community, robust bioinformatics standards remain to be established. Here we used *in silico* mock viral communities to evaluate the viromic sequence-to-ecological-inference pipeline, including (*i*) read pre-processing and metagenome assembly, (*ii*) thresholds applied to estimate viral relative abundances based on read mapping to assembled contigs, and (*iii*) normalization methods applied to the matrix of viral relative abundances for alpha and beta diversity estimates.

Results. Tools specifically designed for metagenomes, specifically metaSPAdes and MEGAHIT, were the most effective at assembling viromes. Read pre-processing, such as partitioning, had virtually no impact on assembly output, but may be useful when hardware is limited. Viral populations with 2–5x coverage typically assembled well, whereas lesser coverage led to fragmented assembly. Strain heterogeneity within populations hampered assembly, especially when strains were closely related (average nucleotide identity, or ANI ≥ 97%) and when the most abundant strain represented < 50% of the population. Viral community composition assessments based on read recruitment were generally accurate when the following thresholds for detection were applied: (*i*) ≥ 10kb contig lengths to define populations, (*ii*) coverage defined from reads mapping at ≥ 90% identity, and (*ii*) ≥ 75% of contig length with ≥ 1x coverage. Finally, although data are limited to the most abundant viruses in a community, alpha and beta diversity patterns were robustly estimated (±10%) when comparing samples of similar sequencing depth, but more divergent (up to 80%) when sequencing depth was uneven across the dataset. In the latter cases, the use of normalization methods specifically developed for metagenomes provided the best estimates.

Conclusions. These simulations provide benchmarks for selecting analysis cut-offs and establish that an optimized sample-to-ecological-inference viromics pipeline is robust for making ecological inferences from natural viral communities. Continued development to better accessing RNA, rare, and/or diverse viral populations and improved reference viral genome availability will alleviate many of viromics remaining limitations.

Keywords

Virus / Virome / Viral Ecology / Metagenome / Assembly / Benchmarks

Background

Microbial communities and their associated viruses are abundant, diverse, and play key roles in
50   Earth's ecosystems and processes (Falkowski, Fenchel & Delong, 2008; Cobián Güemes et al., 2016).
However, because most microbes and viruses remain uncultivated, and because viruses do not harbor a
universal marker gene, viral ecology studies remain challenging to perform (Brum & Sullivan, 2015;
Solden, Lloyd & Wrighton, 2016). Viral metagenomics (viromics) is a uniquely powerful tool for high-
throughput analysis of uncultivated viruses (Brum & Sullivan, 2015; Cobián Güemes et al., 2016).
55   Initial viromics studies, despite being limited to gene-level analyses, revealed the large diversity of
viral-encoded genes (Edwards & Rohwer, 2005; Schoenfeld et al., 2008), provided first estimates of
richness and functional diversity across natural viral communities (Hurwitz, Hallam & Sullivan, 2013;
Hurwitz, Brum & Sullivan, 2015), and suggested the existence of biome-specific viral communities
distributed worldwide (Rodriguez-Brito et al., 2010; Roux et al., 2012).

60   Thanks to recent improvements in high-throughput sequencing technologies and genome assembly,
viromes now also provide the opportunity to assemble large genomes fragments (and even complete
genomes) of uncultivated viruses (reviewed in Brum and Sullivan, 2015; Rose et al., 2016).
Historically, *in silico* benchmarks of the assembly process for microbial metagenomes indicated that
accurate bacterial and archaeal genomes (complete or partial) could be recovered for relatively
65   abundant lineages given sufficient sequencing depth, but revealed potential issues including
misassemblies deriving from the presence of very closely related organisms (Mavromatis et al., 2007;
Mende et al., 2012; Greenwald et al., 2017; Sczyrba et al., 2017). Viral community datasets are
typically processed using the same methodologies, and viral-specific benchmarks came to a similar
conclusion: viral genomes can be assembled from metagenomes, but the presence of co-existing viruses
70   with highly similar regions in their genome can lead to reduced contig size and/or chimeric contigs
(Aguirre de Cárcer, Angly & Alcamí, 2014; Vázquez-Castellanos et al., 2014; García-López, Vázquez-
Castellanos & Moya, 2015; Martinez-Hernandez et al., 2017; White, Wang & Hall, 2017). However,
new metagenome assembly softwares (e.g. metaSPAdes (Nurk et al., 2017)) and methods for read
filtering and/or partitioning prior to assembly (e.g. khmer (Crusoe et al., 2015)) that might improve
75   assembly quality have yet to be evaluated with viral data.

For bacteria and archaea, advances in genome binning and genome validation approaches (e.g.,
(Parks et al., 2015)) have significantly improved the recovery of accurately reconstructed genomes
from increasingly complex environments (Wrighton et al., 2012; Sharon et al., 2013; Waldor et al.,
2015; Sangwan, Xia & Gilbert, 2016; Sczyrba et al., 2017). These methods rely on single-copy marker
80   genes to assess genome bin completeness and "contamination" (i.e. multiple genomes in the same
genome bin), two metrics critical to guide the optimization of genome binning parameters and curate
the final dataset (Parks et al., 2015; Bowers et al., 2017). Unfortunately, because of the absence of
universal single-copy viral marker gene, viral genome bins are much more challenging to interpret and
analyze. Since viral genomes are also smaller than microbial ones and thus more frequently assembled
85   in a single contig, viromics studies usually rely on the assembled contigs without applying any genome
binning step.

For ecological analyses, a community abundance matrix of microbial OTU counts across samples is
the typical starting point, and this "OTU table" is often derived from 16S rRNA gene abundances in
amplicon sequencing datasets or metagenomes (Hill et al., 2003; Roesch et al., 2007; Fulthorpe et al.,
90   2008; Fierer et al., 2011; Logares et al., 2014). Even for these relatively established microbial
ecological analyses, appropriate normalization methods that account for different sequencing
throughput across samples are still debated, and rarely are results compared across multiple
normalization methods to establish best practices (Doll et al., 2013; Paulson et al., 2013; McMurdie &
Holmes, 2014). This microbial ecology pipeline also needs adjustment when applied to viruses because
95   viruses lack a universal marker gene, precluding amplicon-based viral population abundance estimates
at the community scale (although amplicon-based studies have been successful for ecological analyses

of specific viral lineages, e.g., (Filée et al., 2005; Goldsmith et al., 2011; Chow & Fuhrman, 2012)).
Notably, comparative genomic and ecological analysis of model systems enabled the identification of
sequence-discrete populations, which represent stable ecotypes in natural viral communities (Marston
100   & Amrich, 2009; Gregory et al., 2016; Marston & Martiny, 2016). Thus, in the absence of a universal
viral marker gene, these genome-based populations have been proposed to be used as a viral population
units (akin to a microbial operational taxonomic unit, OTU) in ecological analysis (Brum et al., 2015).
Pragmatically, viral populations are derived from *de novo* metagenomic assemblies, with abundances
estimated by metagenomic read recruitment. Ecological analyses of these contig-derived abundance
105   matrices still have to be comprehensively evaluated, although one bias specific to this approach has
already been identified: counting each assembled contig as a separate OTU can lead to over-estimates
of the number of different viruses in the community (Aziz et al., 2015; García-López, Vázquez-
Castellanos & Moya, 2015).
          Here we used 14 *in silico* simulated viral metagenomes to (*i*) compare the assembly results across
110   different reads pre-processing methods and assemblers, both in terms of the overall genomes recovery
and the number and type of errors observed, (*ii*) assess potential biases and identify optimal thresholds
for identification and quantification of viral populations from metagenomic contigs, and (*iii*) determine
if virome populations abundance matrices can provide reliable estimates of alpha diversity (i.e.
diversity within a community) and beta diversity (i.e. differentiation between communities), even in
115   cases where sequencing depth vary widely (up to two orders of magnitude) between samples.

Methods

Mock community design
120   Viral genomes were randomly selected among the complete genomes of viruses infecting bacteria or
archaea in the NCBI RefSeq database (v69, 2015-02). For each mock community, the total number of
viruses randomly selected (between 500 and 1,000, Table S1), as well as the parameter of the power
law distribution used to model relative abundances (between 1 and 50) were varied. To create patterns
of beta diversity across samples, the 50 most abundant viruses were homogenized within each of four
125   sample groups, *i.e.*, samples within a group shared 30 to 50 of their most abundant viruses, and samples
between groups did not share any of their most abundant 50 viruses. This led to a clear beta diversity
pattern with the mock communities clustering into four groups (Fig. S1F, a PerMANOVA was
performed in R with the package vegan (Oksanen et al., 2008) to verify that the sample groups were
significantly different).
130

Virome simulations
          To simulate virome sequencing for each mock community, the number of reads derived from each
genome was first calculated based on the relative abundance of the genome in the mock community
and the total number of reads sequenced in the virome (10 millions paired-end reads in the initial
135   viromes, 1 million and 100,000 paired-end reads for the subsets at 10% and 1% respectively). Then,
NeSSM (Jia et al., 2013) was used to generate random reads at the prescribed abundances with
simulated Illumina HiSeq errors.

Reads processing
140   Reads generated by NeSSM were first quality-controlled with Trimmomatic (Bolger, Lohse &
Usadel, 2014) with a minimum base quality threshold of 30 evaluated on sliding windows of 4 bases,
and minimum read length of 50. All sets of additionally pre-processed reads were generated from these
quality-controlled (QC) reads using khmer v1.4.1 (Crusoe et al., 2015), following the online protocols
(http://khmer-protocols.readthedocs.io/, Fig. S2). First, a dataset of digitally normalized reads was
145   generated, i.e. a dataset in which all reads with median k-mer abundance higher than a specified

threshold were eliminated. This was done in two steps by normalizing k-mer coverage first to 20x then to 5x (script "normalize-by-median", dataset "Digital normalization"). The script "do-partition" was then used to partition these digitally normalized datasets, i.e. separate reads that did not connect to each other in the k-mer graphs in different bins (dataset "Partitioned reads (normalized)"). These reads
150   partitions were then re-inflated, i.e., the original abundance of reads was restored to its value prior to digital normalization, with the script "sweep-reads" (dataset "Partitioned reads (inflated)"). Finally, three sets of reads were generated by trimming all low-abundance k-mers for highly covered reads, i.e., highly covered reads (in this case, $\geq$ 20x) were truncated at the first occurrence of a k-mer below a given abundance cutoff (here $\leq$ 2x, $\leq$ 5x, and $\leq$ 20x for the three datasets "Low k-mer filter (2x)",
155   "Low k-mer filter (5x)", "Low k-mer filter (20x)", respectively). This was done with the script "filter-abund", with option "variable-coverage" as recommended for metagenomes.

Assembly and comparison to input genomes

The different read sets were assembled with five different assembly software tools, using
160   metagenomic-optimized parameters (when available, Fig. S2). IDBA-UD v.1.1.1 (Peng et al., 2012) was used with the option "pre-correction" and from fasta reads (converted from fastq reads with the tool "fq2fa"). MetaSPAdes assemblies (Nurk et al., 2017) were computed from the software version 3.10.0, with the option "metagenomic" (all other options default). MEGAHIT assemblies (Li et al., 2016) were computed from version v1.0.6 with presets "meta" (all other options default). MetaVelvet
165   assemblies (Namiki et al., 2012) were computed with software version 1.2.07 with the "discard_chimera" option selected, default parameters otherwise. Omega assemblies (Haider et al., 2014) were computed with software version 1.0.2 and minimum overlap length of 60. Each assembler was applied to each read pool from each sample (7 read pools x 14 samples = 98 assemblies, Fig. S2), retaining all contigs $\geq$ 500 bp for each assembly (Table S4).
170   Contigs were compared to the input genomes with nucmer (Delcher, Salzberg & Phillippy, 2003) (default options). When $\geq$95% of a contig's length matched an input genome at $\geq$ 90% nucleotide identity, that contig was considered to be a genuine assembly of the input genome. Otherwise, if a contig was similar to multiple genomes but to none over $\geq$ 95% of its length, it was considered a chimera. Circular contigs were detected based on identical 5' and 3' ends, as in (Roux et al., 2014). A
175   circular contig with a length corresponding to $\geq$ 95% of the original genome length was considered a genuine complete genome assembly, while circular contigs covering less than 95% of the original genomes were considered false positives (i.e., incomplete contigs incorrectly predicted as complete genome assemblies). R was used to conduct t-test when comparing rate of chimeric contigs across assemblers and reads pre-processing methods, using the MEGAHIT-QC reads assembly as the control
180   (the set of contigs with the lower number of chimeras).

Generation of the non-redundant pool of population contigs and coverage estimation

Based on the previous benchmarks, the assemblies obtained with metaSPAdes from the QC reads were considered to be the most optimal assemblies and were used in all subsequent benchmarking
185   analyses. Contigs from all samples were clustered with nucmer (Delcher, Salzberg & Phillippy, 2003) at $\geq$ 95% ANI across $\geq$ 80% of their lengths, as in (Brum et al., 2015; Gregory et al., 2016), to generate a pool of non-redundant "population contigs". QC reads from each sample were then mapped to these population contigs with bbmap (http://bit.ly/bbMap), with ambiguous mapping assigned to contigs at random (option ambiguous=random). A custom python script was then used to estimate the number of
190   reads and coverage of each contig.

Alpha and beta diversity estimates

The abundance of each population contig in a given sample was estimated based on the number of reads mapping to that contig, normalized by the contig length (to account for differences in contig /

195   genome size). Beyond the raw read counts (normalized by contig length), five abundance matrices were generated with different library size normalization methods as follow (summarized in Fig. S2):

- "Normalized": counts were divided by the total library size, i.e., the total number of QC reads in the sample, as used for example in (Brum et al., 2015). This approach is also known as "total-sum scaling".

200   - "MGSeq": counts were normalized through cumulative-sum scaling with the metagenomeSeq R package (Paulson et al., 2013). This method was specifically designed for metagenomes in which communities are under-sampled (as is the case in most viral metagenome studies), and will divide counts by a cumulative sum of count to a given percentile (as opposed to dividing by total counts as in "Normalized"). This will minimize the effects of the few highly abundant

205   viruses potentially dominating the community, and introducing biases in relative abundances (Paulson et al., 2013).

- "EdgeR": counts were normalized using scaling factors for libraries designed to minimize the log-fold change between samples for most of the populations, computed with the edgeR R package (Robinson, McCarthy & Smyth, 2009). This method was initially developed for count-

210   based expression data and assumes that the relative abundances of most features (here populations) will not vary between two samples.

- "DeSeq": as with EdgeR, counts were normalized to minimize variations between samples for most populations but with a different underlying model, computed with the DESeq R package (Anders & Huber, 2010). As with EdgeR, this method was initially developed for the detection

215   of differentially expressed features in sequence count data analysis.

- "Rarefied": new counts were generated based on rarefied sets of reads, i.e. quality-controlled reads are subsampled (without replacement) to the smallest number of quality-controlled reads across all samples. Thus, all of the libraries are artificially set to the same size, however some data are "wasted" in the process, i.e., for the more deeply sequenced samples, some

220   observations will not be included in the rarefied counts (McMurdie & Holmes, 2014).

Each abundance matrix was then used to calculate alpha and beta diversity indices, namely the Shannon index, Simpson index, and pairwise Bray-Curtis dissimilarities between samples with a custom perl script. R was used to generate all plots using the ggplot2 package (Wickham, 2009), as well as the NMDS and PerMANOVA analyses, computed with the vegan package (Oksanen et al.,

225   2008). For alpha diversity, we opted to only test indices reflecting community structure (Shannon and Simpson indexes) and not indices predicting sample richness (e.g. Chao estimators (Chao, 1984)), since the latter have been highlighted as not suitable for cases in which rare members of the community are not adequately sampled (Haegeman et al., 2013).

230   **Under-sequencing and strain heterogeneity benchmarks**

To evaluate the impact of under-sequencing on alpha and beta diversity estimates, the same pipeline (assembly with metaSPAdes from QC Reads, selection of population contigs, and estimation of alpha and beta diversity) was applied to datasets in which seven of the 14 samples were under-sequenced. Two levels of under-sequencing were tested, one in which under-sequenced samples were set at 10% of

235   the initial library size (i.e. 1,000,000 reads) and another at 1% of the initial library size (100,000 reads, Table S1).

To evaluate the impact of strain heterogeneity (within-population genomic diversity) on assembly success, a custom perl script was used to simulate strain variations as observed on natural populations of T4-like cyanophages (Gregory et al., 2016), i.e. a set of potentially mutated positions were

240   determined for each new simulated strain gathering all intergenic positions, all third codons positions in protein-coding genes, and all positions in two randomly selected genes (to simulate genes undergoing

diversifying selections). These simulations were based on the mock community "Sample_1", for which every genome was transformed into a population composed of a set of related strains.

For each population, three parameters selected randomly and independently:

245   • The total number of strains was set at 10, 50, or 100 strains simulated
       • The strain divergence, controlled by a "mutation rate", i.e. the ratios of positions mutated within the set of positions identified as "potentially mutated" (see above). The other positions in the genome, not selected as potentially mutated, were mutated at a rate 100 times lower. This "mutation rate" was set at 5%, 10%, or 20%. This led to ANI between the generated strains and

250   the original reference genomes of 97-100%, 95-97%, and 90-95%, respectively.
       • The relative abundance of individual strains within the population, sampled from a power-law distribution. The shape of the distribution was controlled by the power-law parameter, set at 0.1, 1, 10, 100, or 1000. This led to the dominant (i.e. most abundant) strain representing from 1% to 100% of the population.

255   For each population, reads were then simulated with NeSSM (Jia et al., 2013), with the total reads generated for each population calculated based on the input coverage (as for previous simulations), and the number of reads generated from each strain calculated from the strains relative abundance. Reads were then processed as previously, i.e. quality-controlled, partitioned, or filtered, and assembled with the 5 assemblers tested using the same options as for the simulated viromes. Finally, the size of the

260   largest contig recovered for each population was compared to the size of the largest contig recovered for the same genome without strain heterogeneity, to evaluate the impact of strain heterogeneity independently from differences in assembly efficiency between coverage levels, reads processing methods, and assemblers.

265   **Results & Discussion**

Mock communities design

A set of 14 viral communities was designed to provide a gradient of alpha diversity and clear beta diversity patterns (Fig. S1, Table S1 & S2). These communities were composed of 500 to 1,000 genomes (randomly sampled within bacteriophages and archaeal viruses available in NCBI RefSeq

270   v69), with the relative abundance of individual genomes based on power law distributions with varying exponents. Beyond differences in alpha diversity, these communities were also designed to organize into four "ecological" clusters, i.e., four groups of mock communities sharing more genomes within than between groups (Fig. S1). Thus, this simulated dataset allows us to evaluate the ability of virome-based population ecology approaches to recover absolute values of alpha diversity, as well as trends in

275   alpha diversity and beta diversity patterns across samples.

Virome reads were simulated *in silico* with NeSSM (Jia et al., 2013) for each mock community (10,000,000 paired-end Illumina HiSeq reads, 2 x 100bp). Since the number of reads derived from each genome was based on its prescribed relative abundance in the community, 29.1% to 75.2% of the viral genomes in each mock community did not get "sequenced" at all (*i.e.*, did not yield any reads). This

280   was by design to mimic the lack of sampling for rare viruses by current sequencing efforts of environmental samples.

Testing the capacity and accuracy of assembly tools

Given metagenomic sequence data from these 14 mock communities, we first evaluated currently

285   available assembly algorithms. To this end, five assemblers (IDBA-UD (Peng et al., 2012), MEGAHIT (Li et al., 2016), MetaVelvet (Namiki et al., 2012), Omega (Haider et al., 2014), and metaSPAdes (Nurk et al., 2017), all adapted to assemble metagenomic data) were compared to assess their ability to accurately assemble genomes of bacterial and archaeal viruses from viromes (Fig. S2). As expected, each of the assemblers successfully assembled highly covered genomes (10x or higher) and failed to

assemble most low-coverage genomes (2x and lower, Fig. 1A, Fig. S3A). However, MetaVelvet and Omega required higher coverage to assemble viral genomes (~5-10x), while IDBA-UD, MEGAHIT, and metaSPAdes routinely assembled genomes at ~2-5x coverage (Fig. 1A, Fig. S3A). A similar trend was found when observing genome recovery in a single contig (i.e., the percentage of a genome assembled in a single contig, as opposed to the percentage of a genome assembled when cumulating all contigs). Again, IDBA-UD, MEGAHIT, and metaSPAdes were more efficient than MetaVelvet and Omega for assembling large genome fragments at lower read coverage (~2-20x), and metaSPAdes was also better than IDBA-UD and MEGAHIT for assembling low-coverage genomes in a single large contig (Fig. 1B, Fig. S3B).

When comparing individual genome assemblies across the three best assemblers (metaSPAdes, IDBA-UD, and MEGAHIT), no clear differences could be observed in the genome recovery (Fig. S4, correlation coefficients between assemblers > 0.99). However, the percentage of each genome recovered in a single contig was more variable among assemblers (Fig. S4, correlations coefficients: 0.88-0.98). This comparison did not indicate that one assembler would be systematically better than another, but rather that the best assembly for a given genome could come from any of these three assemblers.

Together these comparisons suggest that: (*i*) IDBA-UD, MEGAHIT, and metaSPAdes are currently the best available choices for maximizing assembly of viral contigs from short-read (100 bp) viromes (assembly accuracy discussed below), (*ii*) regardless of the choice of assembly tool, low coverage genomes (< 2x) are under-assembled, and (*iii*) because assembly success varies across genomes and assemblers, multiple tools should be compared to optimally assemble desired target genomes from viromes.

Impact of k-mer-based read filtering and partitioning on assembly

Next, we evaluated how available read pre-processing approaches impacted genome assembly (using approaches from the khmer package and summarized in Table S3 and Fig. S2) (Crusoe et al., 2015). Briefly, beyond the reference dataset of quality controlled reads, the different methods tested were (*i*) trimming of reads based on low-abundance k-mers, i.e., reads are truncated at the first occurrence of a low-abundance k-mer likely originating from sequencing error, (*ii*) digital normalization, i.e., the removal of redundant sequences to normalize genome coverage at or under a specific value (here 5x), and (*iii*) read partitioning, i.e., separate assembly of the disconnected components of the k-mer graph.

Overall, and compared with the effect of the different assembly algorithms, the read pre-processing had a minimal impact on the assembly output (Fig. 1C & D, Fig. S3 C & D with metaSPAdes; the same observations were made with different assemblers in Fig. S5). The main effects observed were that (*i*) digital normalization (treatments "Digital normalization" and "Partitioned reads (normalized)") led to sub-optimal assemblies, likely because differences in coverage above 5x are useful for assemblers to distinguish between related genomes, and (*ii*) trimming of low-abundance k-mers led to sub-optimal assemblies when the threshold used to define low abundance k-mers was close to the threshold used to define "abundant" reads to be trimmed (effect especially noticeable for the 20x filter, Fig. 1C & D). Conversely, partitioning reads and keeping their coverage information (treatment "Partitioned reads (inflated)") or trimming low-abundance k-mers from high coverage reads (with thresholds of 2x and 5x) had little effect on the assembly output, except on low-coverage genomes (< 5x).

Errors and limitations of genome assembly from viromes

Beyond the assembly of low-coverage genomes, which was found to be challenging for all assemblers tested, other errors are known to occur during the *de novo* assembly of viromes.

First, chimeric contigs (i.e., contigs representing artificial constructs assembled from two or more distinct genomes) were generated in each assembly, as previously noted (Aguirre de Cárcer, Angly & Alcamí, 2014; Vázquez-Castellanos et al., 2014; García-López, Vázquez-Castellanos & Moya, 2015).

In our simulated data, these usually represented less than 2.5% of the assembled datasets, and less than 5% of the large contigs ($\geq$ 10kb), but these numbers varied between assemblers and read curation methods (Fig. 2A&B). For all assemblers, reads after digital normalization always yielded more chimeric contigs, which confirmed that the digital normalization step led to sub-optimal assemblies (p-value < 0.01). MEGAHIT systematically produced fewer chimeric contigs than IDBA-UD and metaSPAdes, especially for large ($\geq$ 10kb) contigs (Fig. 2B, p-value < 0.01). Hence, although MEGAHIT did not assemble as many large genome fragments, the fragments that were assembled contained fewer chimeras.

Next, we investigated whether finished and closed viral genomes assemblies could be robustly identified as "circular" contigs, i.e., contigs with matching 5' and 3' ends, as previously suggested (Roux et al., 2014). The ratio of false-positive circular contigs, i.e. circular contigs that represented less than 95% of the original genome and thus likely arose from repeat regions within a genome, was not modified by read pre-processing but was different among assemblers (Fig. 2C). Specifically, 10 to 30% of the circular contigs generated by MEGAHIT and IDBA-UD did not correspond to a complete genome, while metaSPAdes assemblies rarely included any false positive (4 contigs, or <2%, for metaSPAdes assemblies of quality-controlled reads). This suggests that metaSPAdes circular contigs are more likely to correspond to complete genomes and that the "circularization" of a contig cannot be considered as proof of completeness for MEGAHIT and IDBA-UD contigs.

Finally, we evaluated the impact of population strain heterogeneity – i.e., the co-existence of closely related strains with distinct genomes from the same population – on virome assembly. In microbial communities, strain heterogeneity is known to considerably hamper the assembly of the corresponding genomes (Sharon et al., 2015; Martinez-Hernandez et al., 2017; Sczyrba et al., 2017). Population genetic studies of natural viral communities are however challenged by the paucity of cultivated systems that include multiple viral genomic representatives from a single population. Pragmatically, this means that although strain heterogeneity has been observed for specific model systems (Gregory et al., 2016; Marston & Martiny, 2016), community-wide strain variations that would accurately reflect natural viral communities cannot be pulled from these data. Hence, we opted to generate a mock community using the same populations and relative abundances as Sample 1 above, but introduced some level of strain heterogeneity for each population by varying a combination of 3 parameters: (*i*) the number of strains in the population, either low (n=10), medium (n=50), or high (n=100), (*ii*) the diversity of these strains, presented as the average ANI of strains compared to the consensus population genome, either low (90-95%), medium (95-97%), or high (97-100%), and (*iii*) the evenness of the power-law distribution of strain frequency in the population, either low (dominant variant represents 75-100% of the population), medium (dominant variant 50-75%), or high (dominant variant < 25%). For each genome, reads were thus not generated from the reference genome sequence as before, but from a set of strains generated and sampled using a random combination of these 3 parameters. Then, the same pipeline of read processing and assembly was applied, and the size of the largest contig obtained for each population was compared to the size of the largest contig obtained in the previous mock community assembly (i.e. without strain heterogeneity, Fig. 2D and Fig. S6).

An ANOVA was performed on the complete dataset (i.e. all combinations of assemblers and read processing) to evaluate which component of strain heterogeneity impacted the assembly process (see Methods). The three parameters (number of strains, strain diversity, and evenness of strain distribution) significantly but differently impacted the assembly: population shape (i.e., strain distribution) was the main explanatory variable of suboptimal assemblies (F-value 149.8, p-value<1e-16), strain diversity was also a strong driver of assembly failures (F-value 70.4, p-value<1e-16), while the number of strains in the populations had a more marginal effect (F-value 2.8, p-value 0.06). Overall, when compared to the assemblies generated without strain heterogeneity, contigs were shorter for populations with an even strain distribution (i.e. dominant strain $\leq$ 50% of the population) and/or when strains were more similar to the consensus genome (i.e. average ANI to consensus $\geq$ 97%) and to each other, with

the combination of both leading to the greater reduction in contig length (Fig. 2D). These results indicate that strain heterogeneity within natural viral populations will likely be a key factor contributing to assembly success and failure, and populations of evenly distributed closely related strains will be the most likely to fail to assemble in virome studies.

Population identification and quantification

In viral ecological studies, the next step after assembly often consists of identifying viral populations (i.e. contigs representing individual populations) and quantifying their relative abundances in each sample. We opted to use the contigs assembled with metaSPAdes from quality-controlled reads, as they represented the largest contigs overall across the different samples (despite ~1% chimerism). We pooled contigs generated from all samples into a single non-redundant database (contigs were clustered at ≥ 95% of nucleotide identity across ≥ 80% of the contig length, in accordance with population genome analysis (Gregory et al., 2016)). Quality-controlled reads were then mapped to this database to estimate contig coverage across the 14 samples. Two types of thresholds were evaluated in this mapping step: (*i*) minimum nucleotide identity for a given read to be considered mapped to a given contig, and (*ii*) minimum length of the contig covered to consider a contig as "detected" in a sample (Fig. S2). Reads not meeting the threshold were removed from abundance counts, and contigs not meeting the detection threshold in a given sample were given abundance values of zero for that sample in the resulting coverage table.

Considering all non-redundant contigs ≥ 500 bp as different populations, we observed that increasing the two thresholds (read mapping identity percentage and length of contig covered) progressively decreased the sensitivity of the analysis (evaluated here as the percentage of genomes recovered, Fig. 3A) and the false discovery rate (or FDR, which is the percentage of contigs recovered that were not part of the initial community, Fig. 3B). However, because FDR decreased more precipitously than sensitivity, there is an optimal combination of thresholds for which FDR can be minimized and sensitivity maximized. In these simulations, that optimal threshold was ≥ 75% on the contig length coverage associated with ≥ 90% nucleotide identity for the read mapping, which led to a 3% decrease in sensitivity (compared to the most permissive thresholds), but only 13% FDR (compared to 49% for the most permissive thresholds).

As noted by previous studies (Aziz et al., 2015; García-López, Vázquez-Castellanos & Moya, 2015), considering all non-redundant contigs as distinct populations strongly over-estimated the total number of populations (on average, 2 to 3 contigs were counted for each individual genome, Fig. 3C). Thus, we re-analyzed our dataset using only non-redundant contigs ≥ 10kb or circular as was proposed previously, and as required for taxonomic classification by gene content network-based analysis (Bolduc et al., 2017). Again, the optimal threshold combination was ≥ 75% of the contig length covered and ≥ 90% read mapping identity (Fig. 3 panels D,E, & F). However, while sensitivity declined slightly (~15%) compared to the dataset including all contigs ≥ 500bp, FDR improved drastically to 0.2%, compared to 13% observed in the above analyses. Further, by increasing the stringency of the population definition, the number of contigs per genome that were counted as a population was 1.2 which is much closer to the correct number of 1 contig per genomne. More generally, increasing this contig size threshold quickly decreased the number of contig observed per genome, and most of the over-estimation observed earlier seemed to arise from contigs < 5kb (Fig. S7).

In summary, we recommend that viral populations (as an operational taxonomic unit) be defined and analyzed in viromes using contigs that are ≥ 10 kb or circular, and only considered "detected" when the contig is covered over ≥ 75% of its length by read mapping at ≥ 90% nucleotide identity. However, we also anticipate that the data from these sensitivity analyses will help researchers tune these thresholds to match a given study's need for high sensitivity or low FDR.

Alpha and beta diversity estimation from virome-derived populations

We next sought to evaluate how the variation in community structure of our 14 mock community metagenomes impacted diversity estimations, and did so using our recommended optimized population cut-offs for identifying populations and then estimating their abundances by read mapping. These
440   population count matrices (counting either base pairs or reads mapped to each population contig) were used as input for alpha and beta diversity estimations and compared across the dataset. Notably, these matrices included only a fraction (10-33%) of the original genomes in the dataset, as rare viral genomes were not "sequenced", and low-coverage genomes produced only small (< 10 kb) contigs (Fig. 4A).

Before calculating any index, the read counts were first normalized by the contig length, since viral
445   genome lengths can be highly variable (~2 orders of magnitude, (Angly et al., 2009)). Then, to account for potential differences in library sizes, we compared five different methods: (*i*) a simple normalization in which counts are divided by the library size, "Normalized" (*ii*) a method specifically designed to account for under-sampling of metagenomes, from the metagenomeSeq R package, "MGSeq" (*iii and iv*) two methods designed to minimize log-fold changes between samples for most of
450   the populations, from the edgeR R package, "edgeR", and the DESeq R package, "DESeq", and (*v*) a rarefaction approach whereby all libraries get randomly down-sampled without replacement to the size of the smallest library, "Rarefied" (Fig. S2).

For both Shannon and Simpson alpha diversity indices, the values calculated from normalized count matrices were within 10% of the actual value calculated from the whole community (Fig. 4B & C).
455   Hence, the recovery of abundant members of the community seems to be enough to estimate alpha diversity values. Since both Shannon and Simpson indices are based on the relative abundance of individual members of the community, the three methods that applied a sample-wide correction factor (normalization by library size, MGSeq, EdgeR) all led to the same estimations, while rarefied count matrices and DESeq, which can (slightly) modify relative abundance of populations within
460   communities, provided statistically indistinguishable estimates (Fig. 4 B & C). Similarly, for beta diversity estimates, pairwise Bray-Curtis dissimilarities between samples calculated from normalized counts matrices were highly similar to the dissimilarities calculated from the whole communities for all normalization methods (within 15% of actual values, p-value≤0.001 for Mantel test comparing true and estimated dissimilarity matrices, Fig. 4D). Thus, as long as the count matrices were normalized to
465   account for different contig lengths and library sizes, each of the five methods tested here provided reliable estimates of alpha and beta diversity.

Impact of under-sequencing and possible corrections

Finally, to help guide researchers in making decisions about under-sequenced samples, we evaluated
470   how alpha and beta diversity estimates were impacted by such samples in a dataset. Specifically, we performed the same computations (assembly with metaSPAdes from quality-controlled reads, generation of a pool of dereplicated population contigs, mapping of quality-controlled reads and computation of normalized count matrices), but we did so with a dataset in which half of the samples were drastically under-sequenced either at 10% (subset_10) or 1% (subset_1) of the original
475   sequencing depth, respectively (Table S1, Fig. S2).

Not surprisingly, under-sequenced samples resulted in fewer genomes detected (t-test, p-value < 1e-05, Fig. 4A). Using the same five normalization methods to account for these differences in sequencing depth, we found that the diversity estimations were impacted. The subset_10 samples resulted in Shannon and Simpson estimations that were close (within 16%) to the initial estimates, but the
480   diversity estimates in the subset_1 samples varied as much as 30% (Fig. 4 B & C). Hence, although the different normalization methods tested here helped to compensate for some degree of under-sequencing, none was able to recover the correct values of alpha diversity when sequencing depth was highly variable and/or when some samples were significantly under-sequenced.

Similarly, beta diversity patterns (evaluated as pairwise Bray Curtis dissimilarities) were not
485   estimated as accurately with the under-sequenced samples than with the initial samples: dissimilarities

estimated from subset_10 samples varied as much as 61% compared with the true dissimilarities (mean: 5.9%), and the ones estimated from subset_1 samples varied as much as 77% (mean: 4.4%; Fig. 4 E & F). Rarefaction and MGSeq were the two normalization methods most efficient at limiting these biases, as they led to maximum variations of 11.5% and 11.3% for subset_10, and 10.9% and 52.7% for subset_1, respectively. Moreover, even with the subset_1 samples, the results of an NMDS based on these normalized count matrices were still strongly correlated with the results of an NMDS based on true relative abundances (Fig. S8, $r^2 > 0.9$ for all normalization methods but "rarefied", for which the positions of two groups are switched leading to a lower r^2 of 0.64). Hence, beta diversity trends can be recovered even when sequencing depth was highly variable.

Current limitations of the sample-to-ecological-inference pipeline

Overall, these benchmarks confirmed that virome-derived abundance matrices can be used in ecological studies, with two main caveats. First, absolute viral richness will likely be under-estimated, because the assembly will only yield large contigs for abundant viral genotypes without evenly distributed and/or closely related strains. Hence, absolute values of richness and diversity should be interpreted with care, although once normalized, sample comparisons of these richness and diversity metrics are generally robust to differences in community complexity and sequencing depth. Second, because this approach relies on coverage as a proxy for relative abundance, only quantitative (or near-quantitative) datasets can be used as input (Duhaime et al., 2012). Notably, protocols to generate these quantitative viromes are currently available only for dsDNA and/or ssDNA viruses (Duhaime et al., 2012; Roux et al., 2016), and still remain to be developed for their RNA counterparts, although these RNA viruses might represent up to half of the viral particles in some environments (Steward et al., 2013). Thus, when interpreting viromics-based ecological studies, it is important to remember and clearly state that these reflect only the sub-part of viral communities with (ds)DNA genomes.

Conclusions

Our comparative analysis of 14 simulated viromes showed that the genome-assembly-to-ecological-inference viromics pipeline can efficiently and robustly identify abundant viruses and recover trends in alpha and beta diversity. As viromics becomes routine in viral ecology, the approaches underlined here (both the tools and thresholds used) offer an initial set of "best practices" for data analysis.

Moving forward, increased library size and number associated with improved genome recovery from metagenomes will undoubtedly lead to an unprecedented catalog of uncultivated viral genomes (e.g. 125,000 released in a single study (Paez-Espino et al., 2016)). These will be complemented by viral genomes obtained from other methods, such as single-virus sequencing, which can access less dominant viruses and those with high strain heterogeneity (Martinez-Hernandez et al., 2017). As standards emerge, such uncultivated viral genomes will migrate toward specifically-designed databases (e.g. IMG/VR (Paez-Espino et al., 2016)), and viral ecological studies will be greatly improved by these centralized reference genome data. Beyond improved references (which will also need to include uncultivated RNA viruses), viromics will need to advance from relative abundance estimations to absolute quantification of viral populations, likely coupled with "ground-truthing" provided by quantitative, lineage-specific molecular methods such as phageFISH, polonies, microarrays, or microfluidic PCR (Tadmor et al., 2011; Allers et al., 2013; Martínez-García et al., 2014). Once in-hand, such approaches should enable researchers to address long-standing questions in the viral ecology field, and more fully bring viruses into predictive ecological models across Earth's ecosystems.
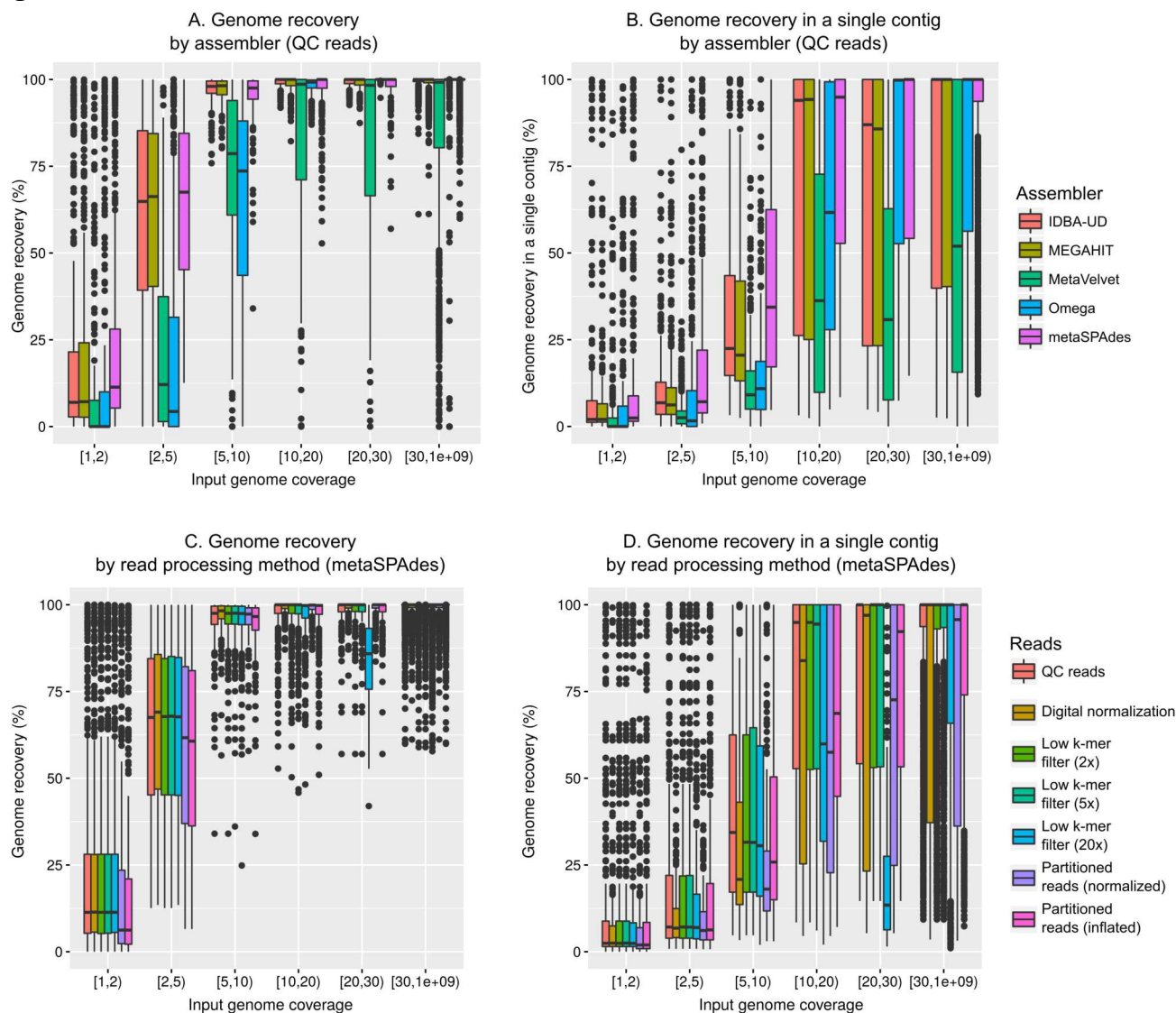
Figures

Figure 1. Influence of assembly software and read curation on genome recovery. All plots display the input coverage on the x-axis, and either the cumulated genome recovery across all contigs (A & C) or the highest genome recovery by a single contig (B & D) on the y-axis. Panels A & B display a comparison of assemblers applied to quality-controlled (QC) reads. Panels C & D present a comparison of read pre-processing methods, all assembled with metaSPAdes. Comparable plots for reads assembled with the other assemblers are available in Fig. S5.
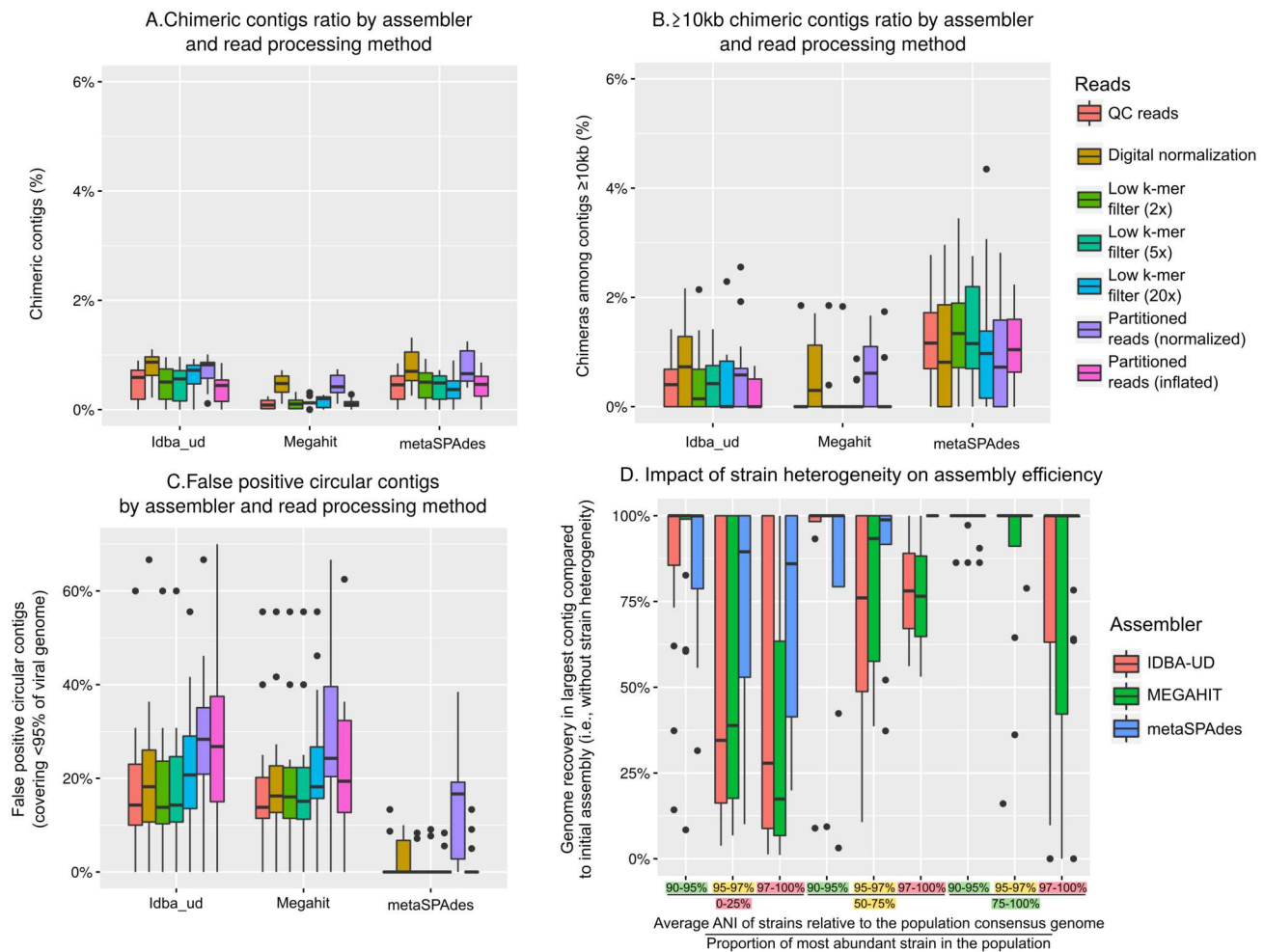
Figure 2. Types and frequency of errors observed in genome assembly from viral metagenomes. A. Percentage of chimeric contigs (i.e. contigs originating from two distinct genomes) across all assembled sequences, by assembler (x-axis) and read curation method (colors). B. Percentage of chimeric contigs among large (≥10kb) contigs, by assembler (x-axis) and read curation method (colors). C. Percentage of false-positive circular contigs, i.e. contigs identified as circular (matching 5' and 3' ends) but representing 95% or less of the original genome, by assembler (x-axis) and read curation method (color). D. Impact of strain heterogeneity (i.e. presence of multiple strains from the same population) on the assembly efficiency. These tests were computed on one mock community (Sample_1), for which each reference genome was replaced with a set of related strains with varying divergence and relative abundances. The y-axis represents the ratio between the largest contig assembled for a genome when strain heterogeneity is introduced and the same parameter without strain heterogeneity (i.e. previous assemblies of the same Sample_1). Populations are grouped based on the two main parameters explaining assembly inefficiency: proportion of the most abundant strain in the population (bottom) and divergence of strains in the population (top). Data presented here include assemblies from QC reads with IDBA-UD, MEGAHIT, and metaSPAdes, while the full set of parameters and approaches tested are presented in Fig. S6.
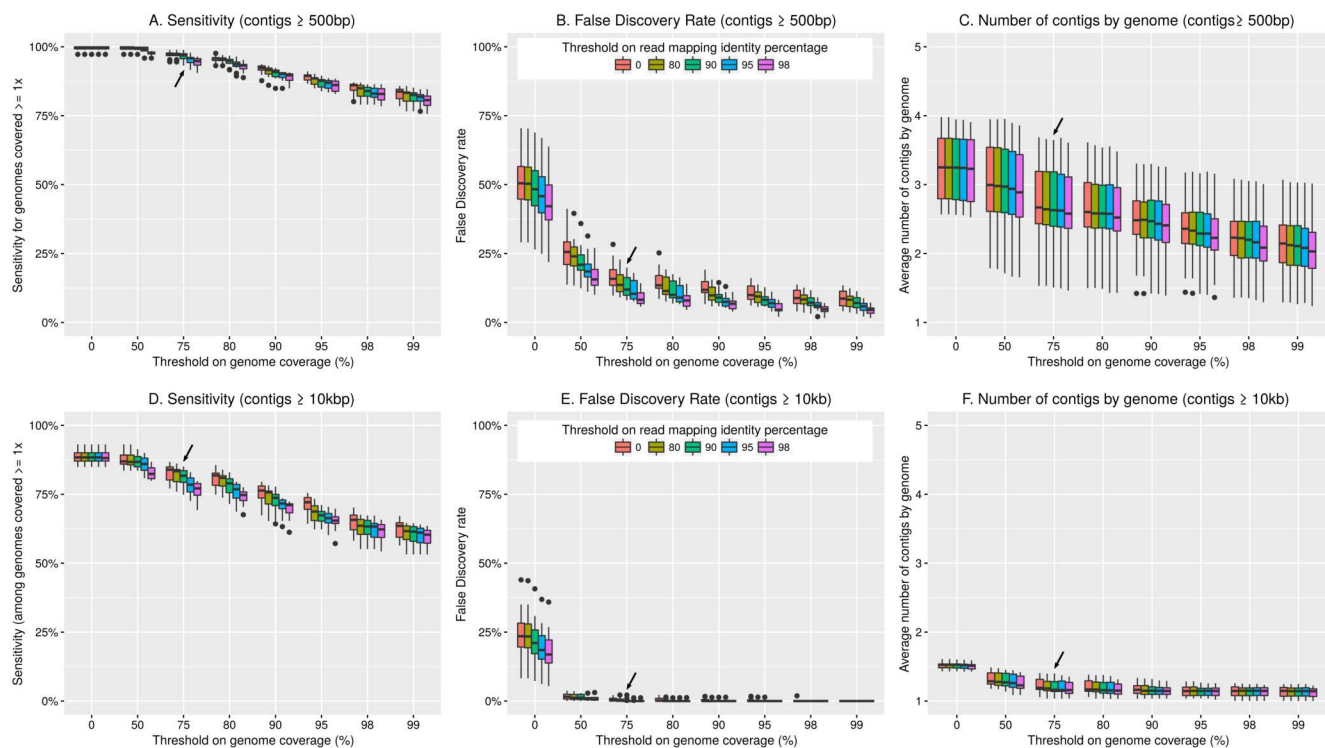
Figure 3. Impact of read mapping thresholds on accuracy of viral population detection. Two parameters were investigated when parsing the mapping of individual virome reads to the population contigs pool: (*i*) the percentage of a contig covered by a sample to considered the contig as detected (x-axis), and (*ii*) the percentage of identity of reads mapping to the contig (color scale). Two pools of population contigs were tested: all non-redundant contigs of ≥ 500 bp (panels A, B, and C), and all non-redundant contigs ≥ 10 kb (panels D, E, and F). Three parameters were observed to evaluate the impact of mapping reads thresholds: the sensitivity of the detection, i.e. percentage of genomes covered at 1x or more in the samples detected through the population contigs mapping (panels A and D), the false-discovery rate which corresponds to the percentage of contigs detected through the population contigs mapping but not associated with any genome from the initial sample (panels B and E), and the average number of population contigs detected for each genome initially covered at 1x or more (panels C and F).
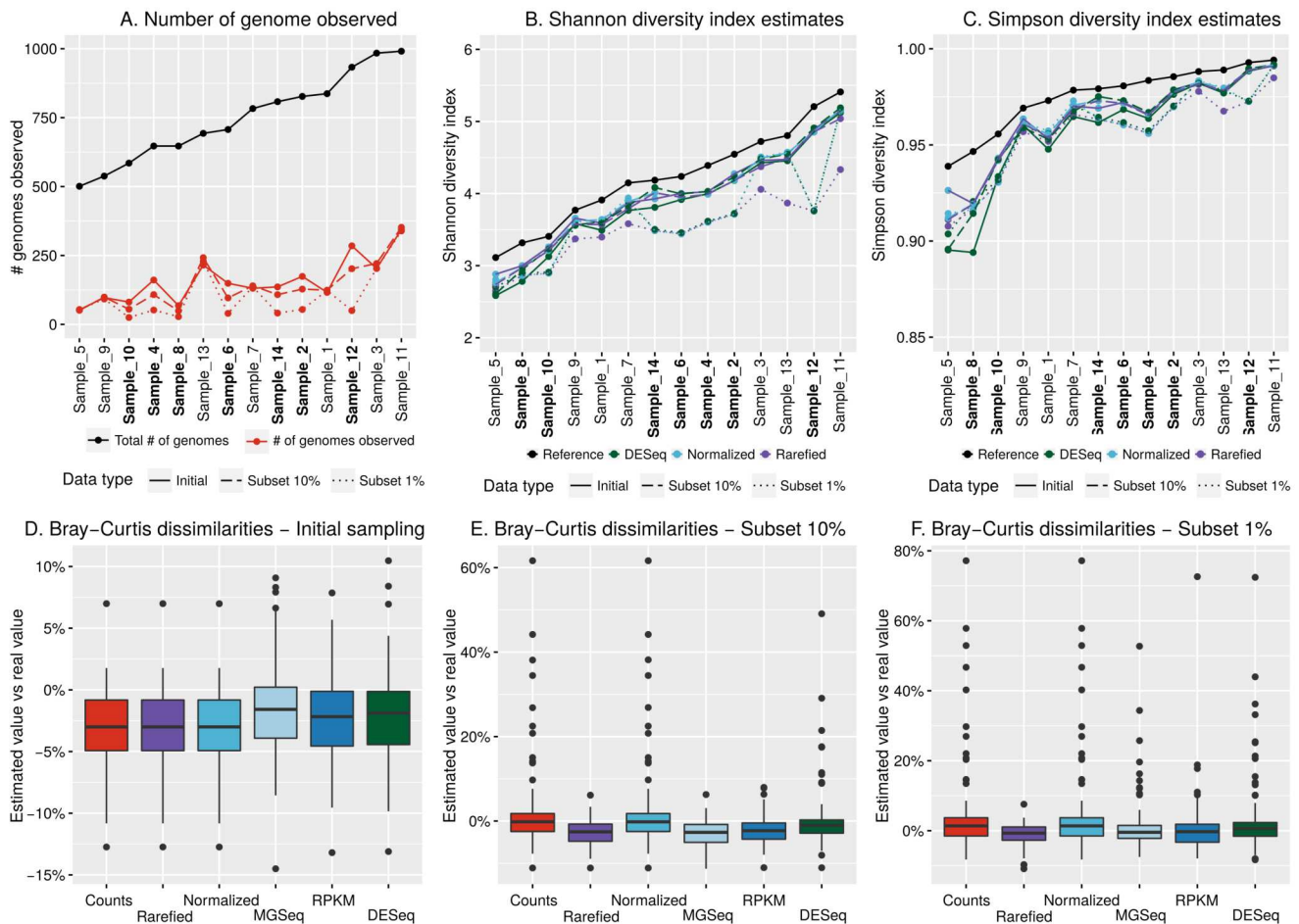
Figure 4. Estimation of alpha and beta diversity from virome-derived viral populations. To
evaluate the impact of varying sequencing depth, six viromes (highlighted in bold in panels A, B, and
C), were sub-sampled at 10% (long dash) or 1% (short dash) of the original read number ("Initial"
corresponds to the assemblies presented in Figure 1, 2, and 3, for which all viromes had the same initial
number of reads). A. Number of genomes observed from the read mapping to viral populations. The
actual number of genomes in the initial simulated community is indicated with black dots, while
estimated based on viromes are colored in red. B. Comparison of Shannon diversity index from the true
community composition (black dots) and estimated from the viromes (colored dots). The different
estimations are based on 3 different normalization methods: counts divided by the total number of
reads sequenced in the virome and the contig size ("Normalized"), counts after rarefying all viromes to
the smallest dataset and normalized by contig size ("Rarefied"), and counts normalized via DESeq
("DESeq"). C. Comparison of Simpson diversity index from the true community composition and
estimated from the viromes (color codes are the same as in panel B). D. Distribution of differences in
Bray-Curtis dissimilarities between samples calculated from true community composition and the same
dissimilarities estimated from the viromes analysis. The different normalization methods (x-axis) are as
follows: counts divided by genome size ("Counts"), counts rarefied to the smallest dataset and
normalized by contig size ("Rarefied"), counts divided by the total number of reads sequenced in the
library and the contig size ("Normalized"), counts normalized by metagenomeSeq ("MGSeq"), EdgeR
("RPKM"), and DESeq ("DESeq"). E. Distribution of differences in Bray-Curtis dissimilarities
between samples calculated from true community composition and the same dissimilarities estimated
from virome analysis, including 6 samples sequenced at 10%. Methods are similar as in panel D. F.
Distribution of differences in Bray-Curtis dissimilarities between samples calculated from true

community composition and from virome analysis, including 6 samples sequenced at 1%. Methods are similar as in panel D.

Supplementary Information

600

Supplementary Figure 1. Characteristics of mock viral communities. Mock communities generated had different number of genomes (panel A) and population distribution (panel B). This led to a range of alpha diversity, as illustrated with Shannon diversity index (C) and Simpson index (D). Mock communities were also designed to display a beta diversity pattern with 4 groups of samples (E and F,
605 BC: Bray-Curtis). The 14 mock communities were designed to cluster into 4 distinct groups, and are colored across all panels according to these 4 groups of significantly similar communities (panel F, PerMANOVA p-value < 0.001).

Supplementary Figure 2. Schematic of the methods evaluated in this study. A. Benchmarking of
610 the assemblers, read pre-processing methods, and thresholds on genome coverage and read mapping identity used to calculate abundance matrices. B. Estimation of the impact of strain heterogeneity on the assembly efficiency. Reference genomes were replaced by populations composed of a set of related strains controlled by 3 parameters. C. Evaluation of the different normalization methods across the three types of datasets, with varying differences in sequencing depth across samples. For all panels, the
615 different methods tested are indicated for each step, and the method and/or threshold chosen or optimal are highlighted in blue (other tests are colored in gray). The metrics used to identify the optimal methods/thresholds are indicated on the left, in green for metrics to maximize, red for metrics to minimize, and black for metrics to compare to "true" data based on whole communities. QC: quality-controlled.

620

Supplementary Figure 3. Influence of assembly software and read curation on genome recovery – dotplots (underlying data for boxplots presented in Figure 1). In these plots, each dot represents the assembly of a single genome in a single sample. A. Genome recovery (i.e. genome coverage by all contigs, y-axis) by genome coverage (x-axis) for different assemblers (colors). B. Genome recovery in
625 a single contig (i.e. genome coverage by the largest assembled contig, y-axis) by genome coverage (x-axis) for different assemblers (colors). C. Genome recovery (i.e. genome coverage by all contigs, y-axis) by genome coverage (x-axis) for different read curation methods (colors). B. Genome recovery in a single contig (i.e. genome coverage by the largest assembled contig, y-axis) by genome coverage (x-axis) for different read curation methods (colors).

630

Supplementary Figure 4. Correlation between assembly results of different assemblers. Top panels display the correlations of genome recovery (i.e. genome coverage by all contigs) for each genome between MEGAHIT and IDBA-UD (A), metaSPAdes and IDBA-UD (B) and metaSPAdes and MEGAHIT (C). Bottom panels display the correlations of genome recovery in a single contig (i.e.
635 genome coverage by the largest assembled contig) for each genome between MEGAHIT and IDBA-UD (D), metaSPAdes and IDBA-UD (E) and metaSPAdes and MEGAHIT (F).

Supplementary Figure 5. Influence of read curation on genome recovery for different assemblers. The assemblers used here are MEGAHIT (A, B), IDBA-UD (C, D), MetaVelvet (E, F), and Omega (G,
640 H). For each assembler, the genome recovery (i.e. genome coverage by all contigs, y-axis) by genome coverage (x-axis) for different read curation methods (panels A, C, E, and G) as well as genome recovery in a single contig (i.e. genome coverage by the largest assembled contig, y-axis) by genome coverage (x-axis) for different read curation methods (panels B, D, F, and H) are displayed. Similar data are displayed for metaSPAdes in Fig. 1 panels C and D.

645

Supplementary Figure 6. Influence of strain-level diversity on assembly efficiency. These tests were computed on one mock community (Sample_1), in which each reference genome was replaced with a set of related strains with varying divergence and relative abundances. In each plot, the y-axis represents the ratio between the largest contig assembled for a genome when strain heterogeneity is

650 introduced and the same parameter without strain heterogeneity (i.e. previous assemblies of the same Sample_1). Plots on the top row display the differences in QC reads assemblies between assemblers, while plots on the bottom row show differences between different reads processing for metaSPAdes assemblies. Populations are grouped based on the different parameters controlling strain heterogeneity, i.e. relative abundance of the dominant strain (left), divergence of the strains (middle), and number of

655 strains in the population (right).

Supplementary Figure 7. Number of population contigs detected for each input genome depending on the minimum contig size threshold for inclusion in population pool. The threshold on contig size used for inclusion in population contigs pools (in bp) is displayed on the x-axis. The

660 distribution of average number of contigs for a given genome (across the samples in which this genome was covered $\geq$ 1x) is displayed on the y-axis.

Supplementary Figure 8. Comparison of NMDS based on viral population counts and the reference mock community composition (reference in top left panel). The different NMDS were

665 computed from the viral population count matrices normalized with the different methods tested in the manuscript (in bold), from the dataset including 6 samples strongly under-sequenced (subset 1%). For each NMDS, the sum of square difference, scaling factor, and significance of the correlation to the reference NMDS is indicated in the plot title (calculated with the function protest from the R package vegan). Samples are colored as in Fig. S1, and an arrow is used to illustrate the difference between the

670 original sample placement in the reference NMDS and the new placement in the NMDS derived from population contigs.

Supplementary Table 1. Mock community design and simulated viromes. Each sample (1 to 14) represents a different mock community, with varying compositions and population structures (Fig. S1).

675 A first virome was simulated for all samples with 20 million reads, and subsets at 2 million and 200,000 reads were also generated for half of the samples.

Supplementary Table 2. Mock community composition. The relative abundance of each genome across the 14 samples is indicated. Viral genomes are identified through their NCBI gi number.

680

Supplementary Table 3. Number of reads retained after each read treatment for initial samples (20 millions raw reads). Treatments are indicated by their code in the first column and detailed in the second column. For read partitioning, the size of each partition (in number of reads) is indicated.

685 **Supplementary Table 4. Assembly statistics for each assembler and each treatment for initial samples.** For each assembly (combination of one sample, one assembler, and one read treatment), the number of contigs, N50, and N80 are indicated.

690 **List of abbreviations**
ANI: Average Nucleotide Identity
ANOVA: ANalysis Of Variance
FDR: False Discovery Rate
NMDS: Non-metric MultiDimensional Scaling
695 OTU: Operational Taxonomic Unit
QC: Quality-controlled (for reads)

Declaration

700 *Ethics approval and consent to participate*
Not applicable

Consent for publication
Not applicable
705

Availability of data and material
The datasets generated for this study are available at
http://datacommons.cyverse.org/browse/iplant/home/shared/iVirus/Virome_pipeline_benchmark
The scripts used in this study are available at
710 https://bitbucket.org/MAVERICLab/benchmarking_viromics

Competing interests
The authors declare that they have no competing interests

Authors' contributions
All authors designed the experiment and contributed to the interpretation of the results and the writing
725 of the manuscript. SR computed the *in silico* simulations and analyses.

References

Aguirre de Cárcer D., Angly FE., Alcamí A. 2014. Evaluation of viral genome assembly and diversity estimation in deep metagenomes. *BMC Genomics 2014 15:1* 15:e368. DOI: 10.1186/1471-2164-15-989.

Allers E., Moraru C., Duhaime MB., Beneze E., Solonenko N., Canosa JB., Amann R., Sullivan MB. 2013. Single-cell and population level viral infection dynamics revealed by phageFISH, a method to visualize intracellular and free viruses. *Environmental Microbiology* 15:2306–18. DOI: 10.1111/1462-2920.12100.

Anders S., Huber W. 2010. Differential expression analysis for sequence count data. *Genome Biology* 11:R106. DOI: 10.1186/gb-2010-11-10-r106.

Angly FE., Willner D., Prieto-Davó A., Edwards RA., Schmieder R., Vega-Thurber R., Antonopoulos DA., Barott K., Cottrell MT., Desnues C., Dinsdale EA., Furlan M., Haynes M., Henn MR., Hu Y., Kirchman DL., McDole T., McPherson JD., Meyer F., Miller RM., Mundt E., Naviaux RK., Rodriguez-Mueller B., Stevens R., Wegley L., Zhang L., Zhu B., Rohwer F. 2009. The GAAS metagenomic tool and its estimations of viral and microbial average genome size in four major biomes. *PLoS computational biology* 5:e1000593. DOI: 10.1371/journal.pcbi.1000593.

Aziz RK., Dwivedi B., Akhter S., Breitbart M., Edwards RA. 2015. Multidimensional metrics for estimating phage abundance , distribution , gene density , and sequence coverage in metagenomes. *Frontiers in Microbiology* 6. DOI: 10.3389/fmicb.2015.00381.

Bolduc B., Jang H Bin., Doulcier G., You Z-Q., Roux S., Sullivan MB. 2017. vConTACT: an iVirus tool to classify double-stranded DNA viruses that infect *Archaea* and *Bacteria*. *PeerJ* 5:e3243. DOI: 10.7717/peerj.3243.

Bolger AM., Lohse M., Usadel B. 2014. Trimmomatic: A flexible trimmer for Illumina sequence data. *Bioinformatics* 30:2114–2120. DOI: 10.1093/bioinformatics/btu170.

Bowers RM., Kyrpides NC., Stepanauskas R., Harmon-Smith M., Schulz F., Doud D., Reddy TBK., Jarett J., Rivers AR., Eloe-Fadrosh EA., Tringe SG., Ivanova N., Copeland A., Clum A., Becraft ED., Malmstrom RR., Birren B., Schriml L., Podar M., Bork P., Weinstock GM., Banfield JF., Garrity GM., Hugenholtz P., Parks DH., Tyson GW., Rinke C., Dodsworth J a., Yooseph S., Sutton G., Yilmaz P., Glockner FO., Meyer F., Gilbert JA., Nelson WC., Hallam SJ., Jungbluth SP., Ettema TJG., Tighe S., Konstantinidis KT., Liu W-T., Baker BJ., Rattei T., Eisen JA., Hedlund BP., Mcmahon KD., Fierer N., Knight R., Finn RD., Karsch-Mizrachi I., Eren A., Woyke T. 2017. Minimum information about a single amplified genome (MISAG) and a metagenome-assembled genome (MIMAG) of bacteria and archaea. *Nature Biotechnology* in press.

Brum J., Ignacio-Espinoza J., Roux S., Doulcier G., Acinas SG., Alberti A., Chaffron S., Cruaud C., de Vargas C., Gasol JM., Gorsky G., Gregory AC., Ogata H., Pesant S., Poulos BT., Schwenck SM., Speich S., Dimier C., Kandels-Lewis S., Picheral M., Searson S., Coordinators TO., Bork P.,

Bowler C., Sunagawa S., Wincker P., Karsenti E., Sullivan MB. 2015. Patterns and ecological
770   drivers of ocean viral communities. *Science* 348:1261498-1–10. DOI: 10.1126/science.1261498.

Brum JR., Sullivan MB. 2015. Rising to the challenge: accelerated pace of discovery transforms marine
       virology. *Nature reviews. Microbiology* 13:1–13. DOI: 10.1038/nrmicro3404.

Chao A. 1984. Nonparametric Estimation of the Number of Classes in a Population. *Scandinavian
       Journal of Statistics* 11:265–70.

775   Chow CET., Fuhrman JA. 2012. Seasonality and monthly dynamics of marine myovirus communities.
       Environmental Microbiology 14:2171–2183. DOI: 10.1111/j.1462-2920.2012.02744.x.

Cobián Güemes AG., Youle M., Cantú VA., Felts B., Nulton J., Rohwer F. 2016. Viruses as Winners in
       the Game of Life. *Annual Review of Virology* 3:197–214. DOI: 10.1146/annurev-virology-100114-
       054952.

780   Crusoe MR., Alameldin HF., Awad S., Boucher E., Caldwell A., Cartwright R., Charbonneau A.,
       Constantinides B., Edvenson G., Fay S., Fenton J., Fenzl T., Fish J., Garcia-Gutierrez L., Garland
       P., Gluck J., González I., Guermond S., Guo J., Gupta A., Herr JR., Howe A., Hyer A., Härpfer A.,
       Irber L., Kidd R., Lin D., Lippi J., Mansour T., McA'Nulty P., McDonald E., Mizzi J., Murray
       KD., Nahum JR., Nanlohy K., Nederbragt AJ., Ortiz-Zuazaga H., Ory J., Pell J., Pepe-Ranney C.,
785   Russ ZN., Schwarz E., Scott C., Seaman J., Sievert S., Simpson J., Skennerton CT., Spencer J.,
       Srinivasan R., Standage D., Stapleton JA., Steinman SR., Stein J., Taylor B., Trimble W., Wiencko
       HL., Wright M., Wyss B., Zhang Q., Zyme E., Brown CT. 2015. The khmer software package:
       enabling efficient nucleotide sequence analysis. *F1000Research* 4:900. DOI:
       10.12688/f1000research.6924.1.

790   Delcher AL., Salzberg SL., Phillippy AM. 2003. Using MUMmer to identify similar regions in large
       sequence sets. *Current protocols in bioinformatics* 00:10.3:10.3.1–10.3.18. DOI:
       10.1002/0471250953.bi1003s00.

Doll HM., Armitage DW., Daly R a., Emerson JB., Goltsman DSA., Yelton AP., Kerekes J., Firestone
       MK., Potts MD. 2013. Utilizing novel diversity estimators to quantify multiple dimensions of
795   microbial biodiversity across domains. *BMC microbiology* 13:259. DOI: 10.1186/1471-2180-13-
       259.

Duhaime MB., Deng L., Poulos BT., Sullivan MB. 2012. Towards quantitative metagenomics of wild
       viruses and other ultra-low concentration DNA samples: a rigorous assessment and optimization
       of the linker amplification method. *Environmental microbiology* 14:2526–37. DOI:
800   10.1111/j.1462-2920.2012.02791.x.

Edwards RA., Rohwer F. 2005. Viral metagenomics. *Nature Reviews Microbiology* 3:504–510.

Falkowski PG., Fenchel T., Delong EF. 2008. The Microbial Engines That Drive Earth's
       Biogeochemical Cycles. *Science* 320:1034–9. DOI: 10.1126/science.1153213.

Fierer N., McCain C., Meir P., Zimmerman M., Rapp JM., SIlman MR., Knight R. 2011. Microbes do not follow the elevational diversity patterns of plants and animals. *Ecology* 92:2013–2019.

Filée J., Tétart F., Suttle CA., Krisch HM. 2005. Marine T4-type bacteriophages, a ubiquitous component of the dark matter of the biosphere. *Proceedings of the National Academy of Sciences of the United States of America* 102:12471–6. DOI: 10.1073/pnas.0503404102.

Fulthorpe RR., Roesch LFW., Riva A., Triplett EW. 2008. Distantly sampled soils carry few species in common. *Isme Journal* 2:901–910. DOI: 10.1038/ismej.2008.55.

García-López R., Vázquez-Castellanos JF., Moya A. 2015. Fragmentation and Coverage Variation in Viral Metagenome Assemblies, and Their Effect in Diversity Calculations. *Frontiers in bioengineering and biotechnology* 3:141. DOI: 10.3389/fbioe.2015.00141.

Goldsmith DB., Crosti G., Dwivedi B., McDaniel LD., Varsani A., Suttle CA., Weinbauer MG., Sandaa R-AA., Breitbart M. 2011. Development of phoH as a novel signature gene for assessing marine phage diversity. *Applied and environmental microbiology* 77:7730–9. DOI: 10.1128/AEM.05531-11.

Greenwald WW., Klitgord N., Seguritan V., Yooseph S., Venter JC., Garner C., Nelson KE., Li W. 2017. Utilization of defined microbial communities enables effective evaluation of meta-genomic assemblies. *BMC Genomics* 18:296. DOI: 10.1186/s12864-017-3679-5.

Gregory AC., Solonenko SA., Ignacio-Espinoza JC., LaButti K., Copeland A., Sudek S., Maitland A., Chittick L., dos Santos F., Weitz JS., Worden AZ., Woyke T., Sullivan MB. 2016. Genomic differentiation among wild cyanophages despite widespread horizontal gene transfer. *BMC Genomics* 17:930. DOI: 10.1186/s12864-016-3286-x.

Haegeman B., Hamelin J., Moriarty J., Neal P., Dushoff J., Weitz JS. 2013. Robust estimation of microbial diversity in theory and in practice. *The ISME journal* 7:1092–101. DOI: 10.1038/ismej.2013.10.

Haider B., Ahn TH., Bushnell B., Chai J., Copeland A., Pan C. 2014. Omega: An Overlap-graph de novo Assembler for Metagenomics. *Bioinformatics* 30:2717–2722. DOI: 10.1093/bioinformatics/btu395.

Hill TCJ., Walsh K a., Harris J a., Moffett BF. 2003. Using ecological diversity measures with bacterial communities. *FEMS Microbiol Ecol* 43:1–11. DOI: FEM1 [pii]\n10.1111/j.1574-6941.2003.tb01040.x.

Hurwitz BL., Brum JR., Sullivan MB. 2015. Depth-stratified functional and taxonomic niche specialization in the "core" and "flexible" Pacific Ocean Virome. *The ISME Journal* 9:472–84. DOI: 10.1038/ismej.2014.143.

Hurwitz BL., Hallam SJ., Sullivan MB. 2013. Metabolic reprogramming by viruses in the sunlit and dark ocean. *Genome biology* 14:R123. DOI: 10.1186/gb-2013-14-11-r123.

840   Jia B., Xuan L., Cai K., Hu Z., Ma L., Wei C. 2013. NeSSM: a Next-generation Sequencing Simulator for Metagenomics. *PloS one* 8:e75448. DOI: 10.1371/journal.pone.0075448.

Li D., Luo R., Liu CM., Leung CM., Ting HF., Sadakane K., Yamashita H., Lam TW. 2016. MEGAHIT v1.0: A fast and scalable metagenome assembler driven by advanced methodologies and community practices. *Methods* 102:3–11. DOI: 10.1016/j.ymeth.2016.02.020.

845   Logares R., Sunagawa S., Salazar G., Cornejo-Castillo FM., Ferrera I., Sarmento H., Hingamp P., Ogata H., de Vargas C., Lima-Mendez G., Raes J., Poulain J., Jaillon O., Wincker P., Kandels-Lewis S., Karsenti E., Bork P., Acinas SG. 2014. Metagenomic 16S rDNA Illumina tags are a powerful alternative to amplicon sequencing to explore diversity and structure of microbial communities. *Environmental Microbiology* 16:2659–2671. DOI: 10.1111/1462-2920.12250.

850   Marston MF., Amrich CG. 2009. Recombination and microdiversity in coastal marine cyanophages. *Environmental microbiology* 11:2893–903. DOI: 10.1111/j.1462-2920.2009.02037.x.

Marston MF., Martiny JBH. 2016. Genomic diversification of marine cyanophages into stable ecotypes. *Environmental Microbiology* 18:4240–4253. DOI: 10.1111/1462-2920.13556.

Martínez-García M., Santos F., Moreno-Paz M., Parro V., Antón J. 2014. Unveiling viral–host interactions within the "microbial dark matter." *Nature Communications* 5:1–8. DOI:
855   10.1038/ncomms5542.

Martinez-Hernandez F., Fornas O., Lluesma M., Bolduc B., Cruz M., Martinez Martinez J., Anton J., Gasol J., Rosselli R., Rodriguez-Valera R., Sullivan MB., Acinas SG., Martinez-Garcia M. 2017. Single-virus genomics reveals hidden cosmopolitan and abundant viruses. *Nature communications* in press.

860   Mavromatis K., Ivanova N., Barry K., Shapiro H. 2007. Use of simulated data sets to evaluate the fidelity of metagenomic processing methods. *Nature methods* 4:495–500. DOI: 10.1038/NMETH1043.

McMurdie PJ., Holmes S. 2014. Waste Not, Want Not: Why Rarefying Microbiome Data Is Inadmissible. *PLoS Computational Biology* 10. DOI: 10.1371/journal.pcbi.1003531.

865   Mende DR., Waller AS., Sunagawa S., Järvelin AI., Chan MM., Arumugam M., Raes J., Bork P. 2012. Assessment of metagenomic assembly using simulated next generation sequencing data. *PLoS ONE* 7. DOI: 10.1371/journal.pone.0031386.

Namiki T., Hachiya T., Tanaka H., Sakakibara Y. 2012. MetaVelvet: an extension of Velvet assembler to de novo metagenome assembly from short sequence reads. *Nucleic acids research* 40:e155. DOI:
870   10.1093/nar/gks678.

Nurk S., Meleshko D., Korobeynikov A., Pevzner PA. 2017. metaSPAdes: a new versatile metagenomic assembler. *Genome Research*. DOI: 10.1101/gr.213959.116.

Oksanen J., Kindt R., Legendre P., O'Hara B., Simpson GL., Solymos P., Stevens MHH., Wagner H. 2008. *The vegan Package*.

875   Paez-Espino D., Chen I-MA., Palaniappan K., Ratner A., Chu K., Szeto E., Pillay M., Huang J.,
            Markowitz VM., Nielsen T., Huntemann M., K Reddy TB., Pavlopoulos GA., Sullivan MB.,
            Campbell BJ., Chen F., McMahon K., Hallam SJ., Denef V., Cavicchioli R., Caffrey SM., Streit
            WR., Webster J., Handley KM., Salekdeh GH., Tsesmetzis N., Setubal JC., Pope PB., Liu W-T.,
            Rivers AR., Ivanova NN., Kyrpides NC. 2016. IMG/VR: a database of cultured and uncultured
880   DNA Viruses and retroviruses. *Nucleic acids research* 45:gkw1030. DOI: 10.1093/nar/gkw1030.

      Parks DH., Imelfort M., Skennerton CT., Hugenholtz P., Tyson GW. 2015. CheckM: assessing the
            quality of microbial genomes recovered from. *Genome Research* 25:1043–55. DOI:
            10.1101/gr.186072.114.

      Paulson JN., Stine OC., Bravo HC., Pop M. 2013. Differential abundance analysis for microbial
885   marker-gene surveys. *Nature methods* 10:1200–2. DOI: 10.1038/nmeth.2658.

      Peng Y., Leung HCM., Yiu SM., Chin FYL. 2012. IDBA-UD: a de novo assembler for single-cell and
            metagenomic sequencing data with highly uneven depth. *Bioinformatics* 28:1420–1428.

      Robinson MD., McCarthy DJ., Smyth GK. 2009. edgeR: A Bioconductor package for differential
            expression analysis of digital gene expression data. *Bioinformatics* 26:139–140. DOI:
890   10.1093/bioinformatics/btp616.

      Rodriguez-Brito B., Li L., Wegley L., Furlan M., Angly F., Breitbart M., Buchanan J., Desnues C.,
            Dinsdale E., Edwards R., Felts B., Haynes M., Liu H., Lipson D., Mahaffy J., Martin-Cuadrado
            AB., Mira A., Nulton J., Pasić L., Rayhawk S., Rodriguez-mueller J., Rodriguez-Valera F.,
            Salamon P., Srinagesh S., Thingstad TF., Tran T., Thurber RV., Willner D., Youle M., Rohwer F.
895   2010. Viral and microbial community dynamics in four aquatic environments. *The ISME journal*
            4:739–51. DOI: 10.1038/ismej.2010.1.

      Roesch L., Fulthorpe R., Riva A., Casella G., Hadwin A., Kent A., Daroub S., Camargo F., Farmerie
            W., Triplett E. 2007. Pyrosequencing enumerates and contrasts soil microbial diversity. *The ISME
            Journal* 1:283–290. DOI: 10.1038/ismej.2007.53.Pyrosequencing.

900   Rose R., Constantinides B., Tapinos A., Robertson DL., Prosperi M. 2016. Challenges in the analysis of
            viral metagenomes. *Virus Evolution* 2:vew022. DOI: 10.1093/ve/vew022.

      Roux S., Enault F., Robin A., Ravet V., Personnic S., Theil S., Colombet J., Sime-Ngando T., Debroas
            D. 2012. Assessing the Diversity and Specificity of Two Freshwater Viral Communities through
            Metagenomics. *PLoS One* 7:e33641.

905   Roux S., Tournayre J., Mahul A., Debroas D., Enault F. 2014. Metavir 2: new tools for viral
            metagenome comparison and assembled virome analysis. *BMC Bioinformatics* 15:1–12.

      Roux S., Solonenko NE., Dang VT., Poulos BT., Schwenck SM., Goldsmith DB., Coleman ML.,
            Breitbart M., Sullivan MB. 2016. Towards quantitative viromics for both double-stranded and
            single-stranded DNA viruses. *PeerJ* 4:e2777. DOI: 10.7717/peerj.2777.

910   Sangwan N., Xia F., Gilbert JA. 2016. Recovering complete and draft population genomes from metagenome datasets. *Microbiome* 4:8. DOI: 10.1186/s40168-016-0154-5.

Schoenfeld T., Patterson M., Richardson PM., Wommack KE., Young M., Mead D. 2008. Assembly of viral metagenomes from yellowstone hot springs. *Applied and environmental microbiology* 74:4164–4174.

915   Sczyrba A., Hofmann P., Belmann P., Koslicki D., Dröge J., Gregor I., Majda S., Fiedler J., Dahms E., Bremges A., Fritz A., Garrido-oter R., Jørgensen S., Shapiro N., Blood PD., Gurevich A., Hansen LH., Sørensen SJ., Chia BKH., Denis B., Froula JL., Wang Z., Egan R., Kang DD., Singer W., Jain C., Strous M., Klingenberg H., Meinicke P., Barton M., Lingner T., Lin H., Liao Y., Silva GZ., Cuevas DA., Edwards RA., Saha S., Vitor C., Renard BY., Hill CM., Pop M., Goeker M.,

920   Kyrpides N., Woyke T., Vorholt J., Rubin EM., Darling AE., Rattei T., Alice C. 2017. Critical Assessment of Metagenome Interpretation – a comprehensive benchmark of computational metagenomics software. *bioRxiv*. DOI: 10.1101/099127.

Sharon I., Morowitz MJ., Thomas BC., Costello EK., Relman DA., Banfield JF. 2013. Time series community genomics analysis reveals rapid shifts in bacterial species, strains, and phage during

925   infant gut colonization. *Genome Research* 23:111–120. DOI: 10.1101/gr.142315.112.

Sharon I., Kertesz M., Hug LA., Pushkarev D., Blauwkamp TA., Castelle CJ., Amirebrahimi M., Thomas BC., Burstein D., Tringe SG., Williams KH., Banfield JF. 2015. Accurate, multi-kb reads resolve complex populations and detect rare microorganisms. *Genome Research* 25:534–543. DOI: 10.1101/gr.183012.114.

930   Solden L., Lloyd K., Wrighton K. 2016. The bright side of microbial dark matter: Lessons learned from the uncultivated majority. *Current Opinion in Microbiology* 31:217–226. DOI: 10.1016/j.mib.2016.04.020.

Steward GF., Culley AI., Mueller JA., Wood-Charlson EM., Belcaid M., Poisson G. 2013. Are we missing half of the viruses in the ocean? *The ISME journal* 7:672–679. DOI:

935   10.1038/ismej.2012.121.

Tadmor AD., Ottesen EA., Leadbetter JR., Phillips R., Gallant JA., Cramer P., Weintraub H., Rich A., Maas S., Platas AA., Hawley DK., Yuzenkova Y., Severinov K., Yano T., Kawabata H., Ueda H., Suzuki T., Scott J., Anant S., Navaratnam N., Nicklen S., Coulson AR., Hamilton CE., Mwangi MM., Dewell S., Papavasiliou FN., Gish W., Miller W., Myers EW., Lipman DJ., Cox J., Mann

940   M., Patt S., Schrey M., Rich A., Williams MA., Mulligan RM. 2011. Probing Individual Environmental Bacteria for Viruses by Using Microfluidic Digital PCR. *Science* 333:58–62. DOI: 10.1126/science.1200758.

Vázquez-Castellanos JF., García-López R., Pérez-Brocal V., Pignatelli M., Moya A. 2014. Comparison of different assembly and annotation tools on analysis of simulated viral metagenomic

945   communities in the gut. *BMC genomics* 15:37. DOI: 10.1186/1471-2164-15-37.

Waldor MK., Tyson G., Borenstein E., Ochman H., Moeller A., Finlay BB., Kong HH., Gordon JI., Nelson KE., Dabbagh K., Smith H. 2015. Where Next for Microbiome Research? *PLoS Biology* 13:1–9. DOI: 10.1371/journal.pbio.1002050.

950   White DJ., Wang J., Hall RJ. 2017. Assessing the Impact of Assemblers on Virus Detection in a De Novo Metagenomic Analysis Pipeline. *Journal of Computational Biology* 24:cmb.2017.0008. DOI: 10.1089/cmb.2017.0008.

Wickham H. 2009. *ggplot2: Elegant Graphics for Data Analysis*. Springer Publishing Company.

Wrighton K., Thomas B., Sharon I., Miller CS., Castelle CJ., VerBerkmoes NC., Wilkins MJ., Hettich RL., Lipton MS., Williams KH., Long PE., Banfield JF. 2012. Fermentation, hydrogen, and sulfur
955   metabolism in multiple uncultivated bacterial phyla. *Science* 337:1661–1666.